JOURNAL OF GEOPHYSICAL RESEARCH, VOL. 106, NO. A3, PAGES 3773–3782, MARCH 1, 2001

Hall magnetohydrodynamic reconnection: The Geospace Environment Modeling challenge

Z. W. Ma and A. Bhattacharjee

Department of Physics and Astronomy, University of Iowa, Iowa City

Abstract. Numerical results are presented on the Geospace Environment Modeling (GEM) reconnection challenge (and its variants) from the Hall magnetohydrodynamics (MHD) code developed at the University of Iowa (UI). Resistivity provides the mechanism for breaking field lines in this study. It is shown that the peak reconnection rate in the quasi-saturated regime is controlled dominantly by ions and has a weak dependence on the resistivity. The reconnection rate is close to those obtained from other particle-in-cell, hybrid, and Hall MHD codes. Some differences between the results from the UI Hall MHD code and other codes are discussed.

1. Introduction

Collisionless magnetic reconnection can be studied numerically in a number of complementary models: fully electromagnetic particle-in-cell (PIC), hybrid (particle ions and electron fluid), and Hall magnetohydrodynamics (MHD). The physical underpinnings as well as the numerical methodologies of these models are quite different, and they span a wide range of scales from the microscopic to the macroscopic. The principle objective of the Geospace Environment Modeling (GEM) reconnection challenge is to compare the predictions of various computer codes based on widely different levels of description for the same set of initial conditions. Such a comparison study is useful not only because it provides a way to benchmark existing computer codes but more significantly because it helps delineate fundamental elements that are shared by the different physical models. This paper reports the results on the GEM challenge (and its variants) obtained by the Hall MHD code developed at the University of Iowa (UI) [*Ma and Bhattacharjee,* 1996].

Hall MHD is a promising model for problems involving collisionless magnetic reconnection. One of the principle points of distinction between resistive MHD and Hall MHD lies in Ohm's law. Whereas resistive MHD relies on the collisional Ohm's law,

$$\mathbf{E}+\frac{\mathbf{v}\times\mathbf{B}}{c}=\eta\mathbf{J}\ , \tag{1}$$

Hall MHD incorporates the generalized Ohm's law,

$$\mathbf{E}+\frac{\mathbf{v}\times\mathbf{B}}{c}=\eta\mathbf{J}+\frac{4\pi}{\omega_{pe}^2}\frac{D\mathbf{J}}{Dt}-\left(\frac{\nabla p}{ne}-\frac{\mathbf{J}\times\mathbf{B}}{nec}\right)+\eta_h\nabla^2\mathbf{J}\ . \tag{2}$$

Paper number 1999JA001004.
0148-0227/01/1999JA001004$09.00

In (1) and (2), $\mathbf{E}$ is the electric field, $\mathbf{B}$ is the magnetic field, $\mathbf{v}$ is the plasma flow velocity, $\mathbf{J}$ is the current density, p is the electron pressure (assumed to be a scalar), n is the electron density, e is the magnitude of the electron charge, $D/Dt\equiv\partial/\partial t+\mathbf{v}\cdot\nabla$ is the total convective derivative, η is the plasma resistivity, and η_h is the "hyperresistivity." On the right of (2) the second term is attributed to finite electron inertia, the third is attributed to the electron pressure gradient, and the fourth is attributed to the Hall current. As the thin current sheet generated in the reconnection layer becomes more localized and intense and its width Δ falls in the range $d_e\equiv c/\omega_{pe}\ll\Delta\lesssim d_i\equiv c/\omega_{pi}$ (where ω_{pe} and ω_{pi} are the electron and ion plasma frequencies, respectively), it is important to retain the effect of the collisionless terms enclosed in parentheses (referred to collectively as the Hall terms) in the generalized Ohm's law (2).

Unlike the resistivity η which multiplies $\mathbf{J}$ in the first term on the right of (1), the last term involving the hyperresistivity η_h multiplies the second-order spatial derivative of $\mathbf{J}$ and can help enhance the numerical stability of a Hall MHD code. However, hyperresistivity is not merely a recipe for numerical stability but can be shown to be generated physically by small-scale tearing dynamics in a current layer [*Bhattacharjee and Hameiri,* 1986; *Strauss,* 1986]. It should be borne in mind that microturbulence in current layers does not necessarily generate anomalous resistivity. For example, small-scale tearing turbulence that preserves magnetic helicity but causes magnetic energy to decay produces hyperresistivity but no anomalous resistivity [*Boozer,* 1986; *Bhattacharjee and Hameiri,* 1986; *Biskamp,* 1993]. Whistler instabilities of a thin current layer have also been shown to produce hyperresistivity [*Drake et al.,* 1994]. Hyperresistivity can cause additional heating, diffuse near-singular currents, and play an important role in controlling the small scales during collisionless reconnection dynamics.

The underlying physics of collisionless reconnection involved in the GEM challenge is discussed in the accompanying overview paper by *Birn et al.* [this issue] and will not be repeated here. We will focus instead on the methodology of Hall MHD and the numerical results obtained from the UI code.

The following is a layout of our paper. In section 2 we present the system of equations underlying the UI Hall MHD code and the geometry of the simulation domain. In section 3 we present two benchmark tests of the code, the first involving the Alfvén-whistler wave dispersion relation, and the second involving the so-called Brio-Wu shock problem [*Brio and Wu,* 1988; *Huba and Lyon,* 1999]. In section 4.1, we report the results of computer runs with the same class of equilibrium profiles and parameters as the GEM challenge except for the density profile, which is significantly broader (initial condition 1). In the context of these runs we discuss the effect of numerical resistivity on the measured reconnection rate and demonstrate that such effects are small in our study. In section 4.2 we present numerical results for the parameters of the GEM challenge (initial condition 2) which is nonstandard because the equilibrium density profile has very strong spatial gradients with a characteristic spatial scale of the order of d_i. (This should be contrasted with the profile discussed in section 4.1, which is characterized by a spatial scale significantly larger than d_i.) We show that the strong density gradient in the GEM challenge equilibrium leads to the development of some rapid physical transients, not seen in the more canonical example discussed in section 4.1. As these transients can eventually lead to the termination of the run owing to a numerical instability, we damp them numerically. The peak reconnection rate in the quasi-saturated state of the damped run is then found to be close to that reported from the PIC and hybrid codes. We conclude in section 5 with a few cautionary remarks which place the GEM exercise in the broader context of other possible initial/boundary conditions and identify some of the remaining challenges.

2. Hall MHD: Equations and Geometry

The Hall MHD simulations reported in this paper are carried out in a rectangular box $-L_x/2 \le x \le L_x/2$, $-L_z/2 \le z \le L_z/2$. The coordinate y is assumed to be ignorable; that is, we impose $\partial/\partial y = 0$ for all times. Then the magnetic field can be represented as

$$\mathbf{B} = \hat{\mathbf{y}} \times \nabla\psi(x,z,t) + B_y(x,z,t)\hat{\mathbf{y}} \ , \tag{3}$$

where $\psi(x,z,t)$ is a flux function.

At $t = 0$ the equilibrium magnetic field is given by

$$B_x = B_0 \tanh(z/\lambda_B) \ , \quad B_y = 0 \ , \quad B_z = 0 \ , \tag{4}$$

with the mass density profile

$$\rho(z) = \rho_0 \mathrm{sech}^2(z/\lambda_\rho) + \rho_\infty \ . \tag{5}$$

In (4) and (5), B_0, λ_B, λ_n, ρ_0, and ρ_∞ are positive constants. When $\lambda_B = \lambda_n$, we obtain the classical Harris sheet solution with constant temperature, which is the equilibrium solution used in the GEM challenge.

The compressible MHD equations are

$$\frac{\partial p}{\partial t} = -\nabla \cdot (\rho \mathbf{v}) \ , \tag{6}$$

$$\frac{\partial}{\partial t}(\rho \mathbf{v}) = -\nabla \cdot \left[\rho \mathbf{v}\mathbf{v} + \left(p + \frac{B^2}{2}\right)\mathbf{I} - \mathbf{B}\mathbf{B}\right] \ , \tag{7}$$

$$\frac{\partial p}{\partial t} = -\nabla \cdot (p\mathbf{v}) - (\gamma - 1)p\nabla \cdot \mathbf{v} \ . \tag{8}$$

In (3)–(8), $\mathbf{I}$ is the unit tensor, $\gamma(= 5/3)$ is the ratio of the specific heats of the plasma, and the variables $\mathbf{x}, \mathbf{v}, t, \mathbf{B}, \rho, p$, and ψ are nondimensionalized as follows: $\mathbf{B}/B_0 \to \mathbf{B}$, $\mathbf{x}/d_i \to \mathbf{x}$, $t/\tau_A \to t$, $\psi \to \psi/B_0 d_i$, $v \to v/v_A$, $\rho \to \rho/\rho_0$, and $p \to p/(B_0^2/4\pi)$, where $\tau_A \equiv d_i/v_A = d_i(4\pi\rho_0)^{1/2}/B_0$ is the Alfvén time and ρ_0 is a constant mass density.

To complete (3) and (6)–(8), we need equations for $\psi(x,z,t)$ and $B_y(x,z,t)$. These equations can be obtained by combining Faraday's induction equation with the generalized Ohm's law (equation (2)). The equation for $B_y(x,z,t)$ is

$$\begin{aligned}\frac{\partial B_y}{\partial t} &= -\nabla \cdot (B_y \mathbf{v} + \mathbf{B} \cdot \nabla v_y + \frac{1}{S}\nabla^2 B_y \\ &\quad - d_i \nabla \left[\nabla \times \left(\frac{\mathbf{J} \times \mathbf{B} - \nabla p}{\rho}\right)\right]_y \\ &\quad + \eta_h \nabla^4 B_y \ ,\end{aligned} \tag{9}$$

where $S \equiv \tau_R/\tau_A$ is the Lundquist number, $\tau_R \equiv 4\pi d_i^2/\eta c^2$ is the resistive diffusion time, and the hyperresistivity η_h has been redefined to make it dimensionless. If we combine Faraday's equation with the y component of (2), we obtain

$$\frac{\partial \psi}{\partial t} = -\mathbf{v} \cdot \nabla\psi + \frac{1}{S} J_y + \frac{d_i}{\rho}(\mathbf{J} \times \mathbf{B})_y - \eta_h \nabla^2 J_y \ . \tag{10}$$

In writing (6)–(10) we assume that the ion pressure gradient can be neglected. We also assume that the electron pressure is a scalar which is violated in many space plasmas but is a common assumption in the Earth's magnetotail and the solar corona. The inclusion of tensor pressure effects in fluid models is complicated by the lack of rigorous closure relations for the off-diagonal elements of the pressure tensor.

Note that in writing (10) we have omitted the electron inertia term in (2). This is because even if we set η to zero in (10), numerical resistivity is still sufficiently large in our code that it overwhelms the effect of electron inertia (for a realistic value of the electron mass). For the simulation results reported in this paper this means that resistivity, and not electron inertia, is the mechanism that breaks field lines.

From (9) and (10) it is clear that the time dependence of B_y plays a important role when the Hall current and electron pressure gradient terms are retained in the dynamical equations. Even if B_y is taken to be zero in the initial state, as in the GEM challenge, it is spontaneously generated by the electron and ion dynamics

in Hall MHD [*Sonnerup,* 1979; *Terasawa,* 1983; *Mandt et al.,* 1994; *Krauss-Varban and Omidi,* 1995; *Ma and Bhattacharjee,* 1996; *Biskamp et al.,* 1997; *Shay and Drake,* 1998; *Hesse et al.,* 1999]. The growth of B_y from the initial state (equation (4)) can be calculated by solving the coupled equations (9) and (10) along with (6)–(8).

3. Tests of the Hall MHD Code

We begin by reporting the results of two numerical tests, recommended by J. D. Huba (private communication, 1999), who also provided us with the test results of the Hall MHD code developed at the Naval Research Laboratory (NRL). Our code results on the tests are in close agreement with the predictions of the NRL code. All dissipation terms, including hyperresistivity, are set to zero in the UI code.

3.1. Test 1: The Alfvén-Whistler Dispersion Relation

We consider the simple equilibrium

$$\rho = 1\ , \quad p = 1\ , \quad \mathbf{v} = 0\ , \quad B_x = 1\ , \quad B_y = B_z = 0\ . \tag{11}$$

Linerarizing the Hall MHD equations about the equilibrium (equation (11)) and assuming plane wave solutions of the form $\exp(ikx - i\omega t)$, we obtain the Alfvén-whistler dispersion relation

$$(\omega^2 - k^2)^2 = \omega^2 k^4\ , \tag{12}$$

where $k = 2\pi m/L_x$ ($m = 1, 2, 3\ldots$). For the run reported here we take $L_x = 0.88$. This choice makes k large even for small values of m and makes the solutions dominantly whistler-like. (In the limit $k \to 0$ the dispersion relation tends to the Alfvén root $\omega/k \to 1$.) Figure 1 shows the comparison of the phase speed determined analytically from the dispersion equation (11) and the numerical results from the Hall MHD code. The top frame in Figure 2 represents the contours of perturbed B_y field in the space-time plane for mode eight ($m = 8$), with maxima indicated by white and minima indicated by dark. The numerical results show the preservation of the plane waveform over a significant space and time domain without distortion. The middle and bottom frames show the amplitude of the B_y field at $t = 10$ and at $t = 0$. The amplitude of the wave is nearly the same in the middle and bottom frames, which is evidence of the low level of numerical dissipation in the UI code. At larger values of m (of the order of and greater than 20), when deviations from the analytical dispersion relation are significant (see Figure 1), distortions of the waveform and amplitude attenuation are more visible.

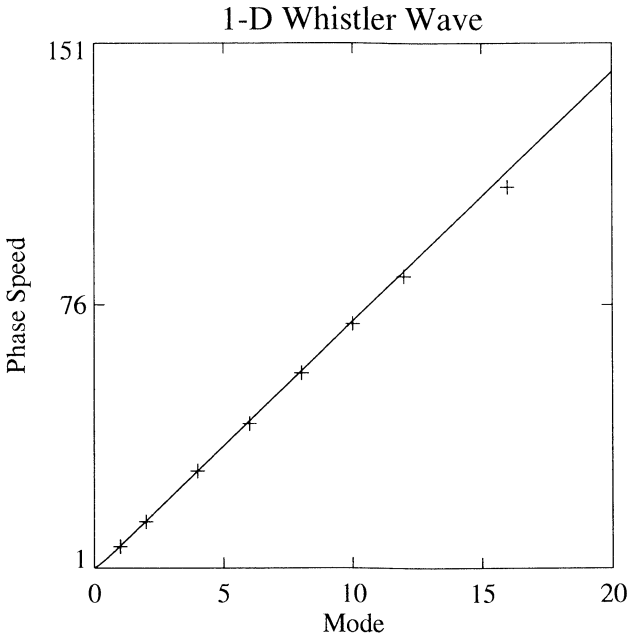

Figure 1. Comparison of the exact analytic Alfvén-whistler dispersion relation (solid line) with numerical results (marked by the pluses) from the University of Iowa (UI) Hall MHD code.

3.2. Test 2: The Brio-Wu Shock Problem

The Brio-Wu shock problem [*Brio and Wu,* 1988; *Huba and Lyon,* 1999] is a Riemann problem which tests whether the UI Hall MHD code can resolve and follow dynamically sharp changes in density, magnetic field, and velocity profiles accurately and without numerical instability. The initial conditions in the plasma density, magnetic B_y field, and v_x are represented by the dashed lines in Figure 3. With these initial conditions, as the system evolves in time, it exhibits fast rarefaction waves (FR), a slow compound wave (SM), a contact discontinuity (CD), and a slow shock (SS). These results are very similar to those produced by the NRL Hall MHD code.

4. Simulation Results on Reconnection

The initial equilibrium state (equation (4)) is driven by a large perturbation given by

$$\psi(x, z) = \psi_0 \cos(2\pi x/L_x) \cos(\pi z/L_z)\ , \tag{13}$$

where $\psi_0 = 0.1$. This perturbation, which is largest at the origin, has been chosen so that the system can attain a nonlinear quasi-saturated state quickly. In what follows we choose $L_x = 25.6d_i$, $L_z = 12.8d_i$, $\lambda_B = 0.5d_i$, and $\rho_\infty/\rho_0 = 0.2$. Simulations are carried out with two sets of initial conditions: (1) a broad density profile with $\lambda_n = 3d_i$ and (2) a narrow density profile with $\lambda_n = 0.5d_i$. Initial condition 2 is the GEM challenge. In the simulations that follow we use 400 grid points with uniform spacing along x and 600 grid points with variable spacing along z. The smallest grid spacing along z is 0.003.

4.1. Initial Condition 1: Broad Density Profile

We first report the numerical results for initial condition 1 with $\lambda_n = 3d_i$. One of the principle consequences of including the Hall current via the generalized Ohm's law is the decoupling of the spatial scales of electron and

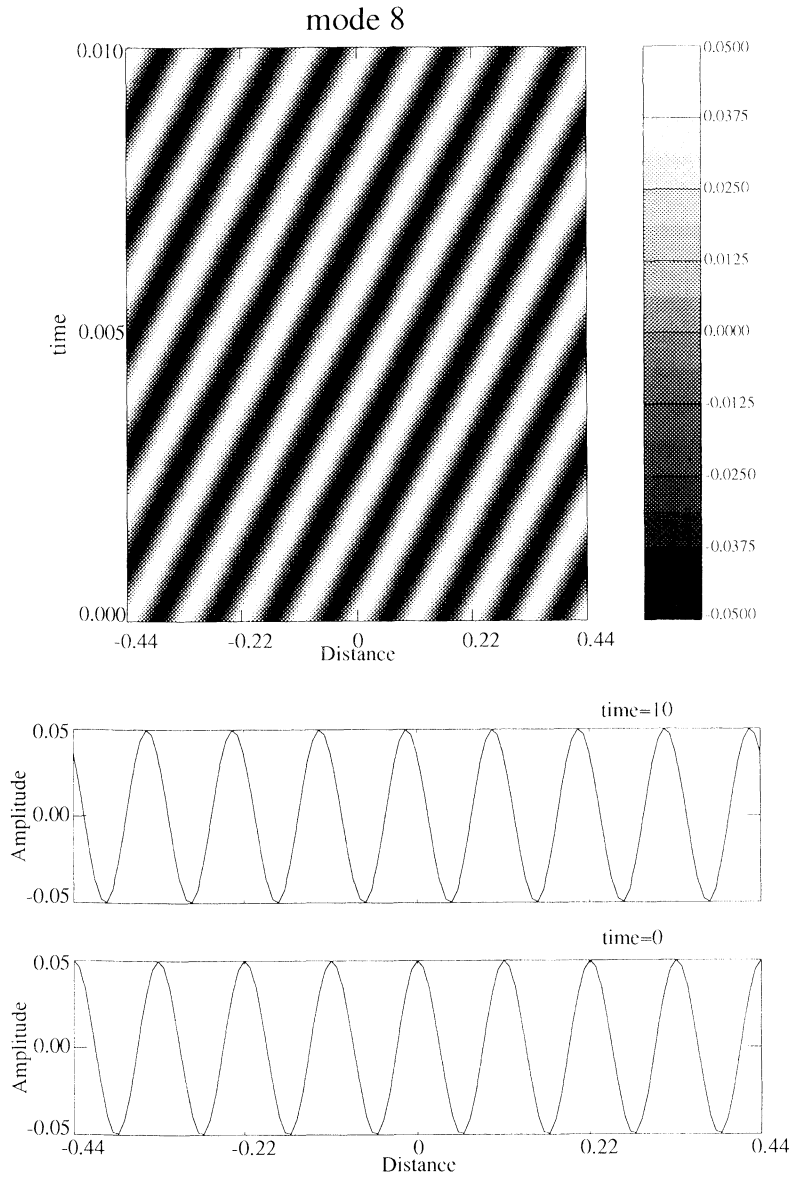

Figure 2. (top) Wave fronts in the space-time domain for Alfvén-whistler waves with mode number $m = 8$. Final (middle) and initial (bottom) amplitudes for a linear Alfvén-whistler wave.

ion dynamics, forbidden in resistive MHD. This leads to a separation of scales between the parallel electric field and current density. Whereas the spatial scale of the parallel electric field transverse to the neutral line is of the order of d_i, that of the parallel current density is determined by the resistivity. This separation of spatial scales is illustrated in Plate 1, which gives the parallel electric field and parallel current density in our simulation at $t = 35$.

The peak value of the reconnection electric field (or equivalently, the reconnection rate) in the quasi-saturated regime is weakly dependent on the resistivity if the value of the resistivity is sufficiently small. For the parameters of initial condition 1 we demonstrate this trend by plotting in Figures 4a and 4b the reconnection rate for different values of S at $t = 35$. (In these runs, hyperresistivity is set to zero.) In Figure 4a the reconnection rate is obtained by calculating ηJ_y at the X point. In Figure 4b the same reconnection rate is obtained from $E_y = d\psi/dt = \partial\psi/\partial t$ (because $\mathbf{v} \cdot \nabla\psi = 0$ at X point). The good quantitative agreement between these two independent methods demonstrates that numerical diffusion in the UI code is low. (If this were not the case, the reconnection rate in Figure 4b would be significantly higher than that in Figure 4a.)

In Table 1 we give the peak reconnection electric field (or reconnection rate) for initial condition 1 runs for different values of the Lundquist number, $S = 100, 200, 250, 300$, and 350. As S increases, the reconnection rate asymptotes to a constant, and the dependence of S becomes weaker. In the regime of high S (low η) the reconnection rate is seen to asymptote to the constant value 0.046.

The ion flow can be calculated by setting $\mathbf{v}_i \approx \mathbf{v}$. In

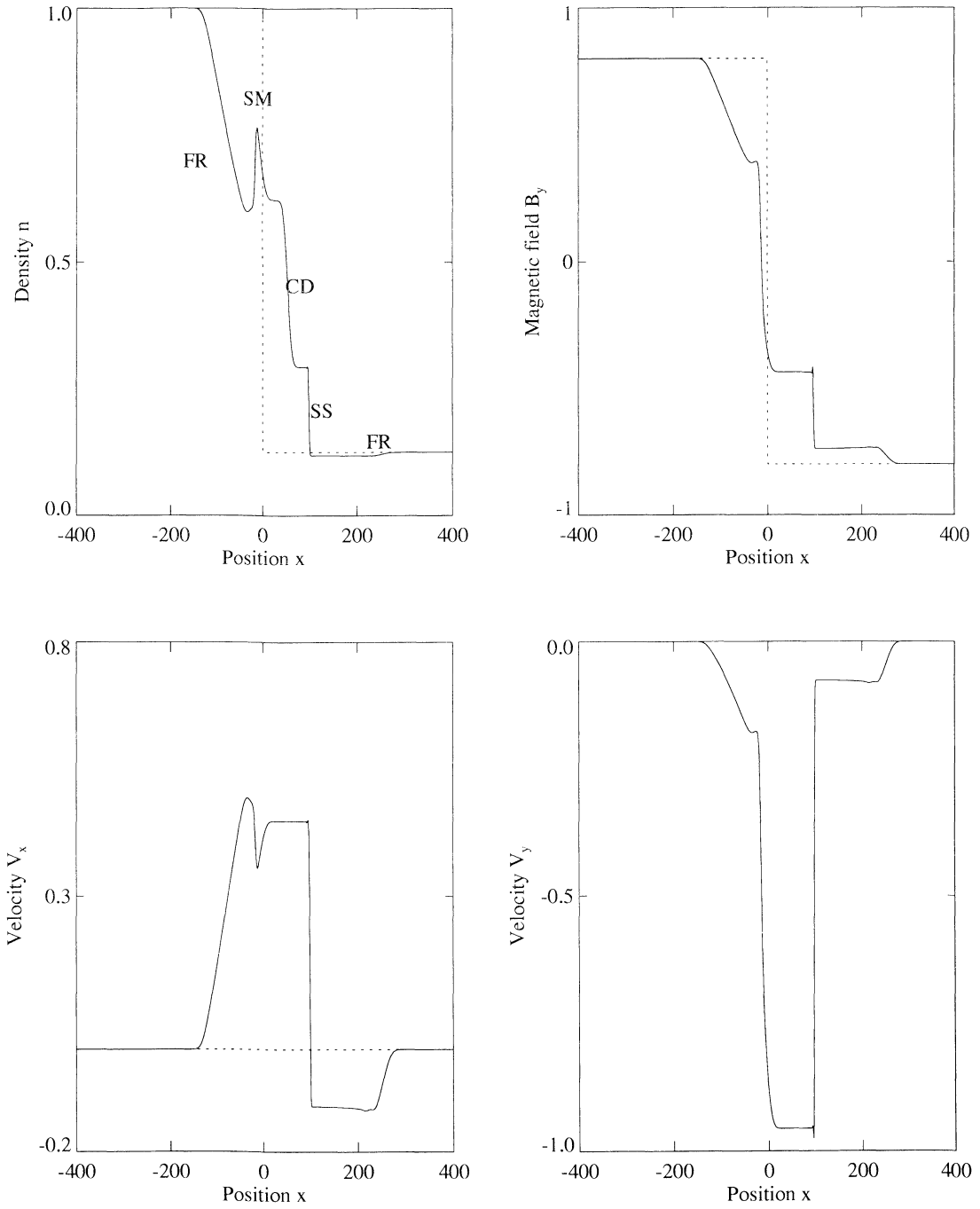

Figure 3. Results for Brio-Wu shock problem from the UI Hall MHD code. The dashed lines represent the initial conditions. SM, a slow compound wave; FR, a fast rarefaction wave; CD, contact discontinuity; SS, slow shock.

the ideal (or outer) region, $|z| \gg d_i$, the electrons and ions move together, and $\mathbf{v}_i \approx \mathbf{v}_e$. The nonideal (or inner region) is composed of two asymptotic regions. In the region $d_i \gtrsim |z| \gg \Delta$ the electrons and ions are decoupled, and $|\mathbf{v}_i| \ll |\mathbf{v}_e|$. In the innermost asymptotic region, $|z| \leq \Delta$, $\mathbf{v}_i \approx 0$, and the current is carried almost completely by electrons. In Plate 2a we plot the (color-coded) contours of $v_x(x, z)$ in the two-dimensional plane for initial condition 1 with $S = 250$ at $t = 35$.

4.2. Initial Condition 2: Narrow Density Profile

We now discuss the numerical results for initial condition 2 with $\lambda_n = 0.5d_i$, which is the GEM challenge. We first report results from a run without any hyperresistivity and numerical damping. Plate 2b shows the (color-coded) contours of $v_x(x, z)$, in this case at $t = 20$ for $S = 200$. Although the maxima and minima of the velocity field in the vicinity of the X point ir

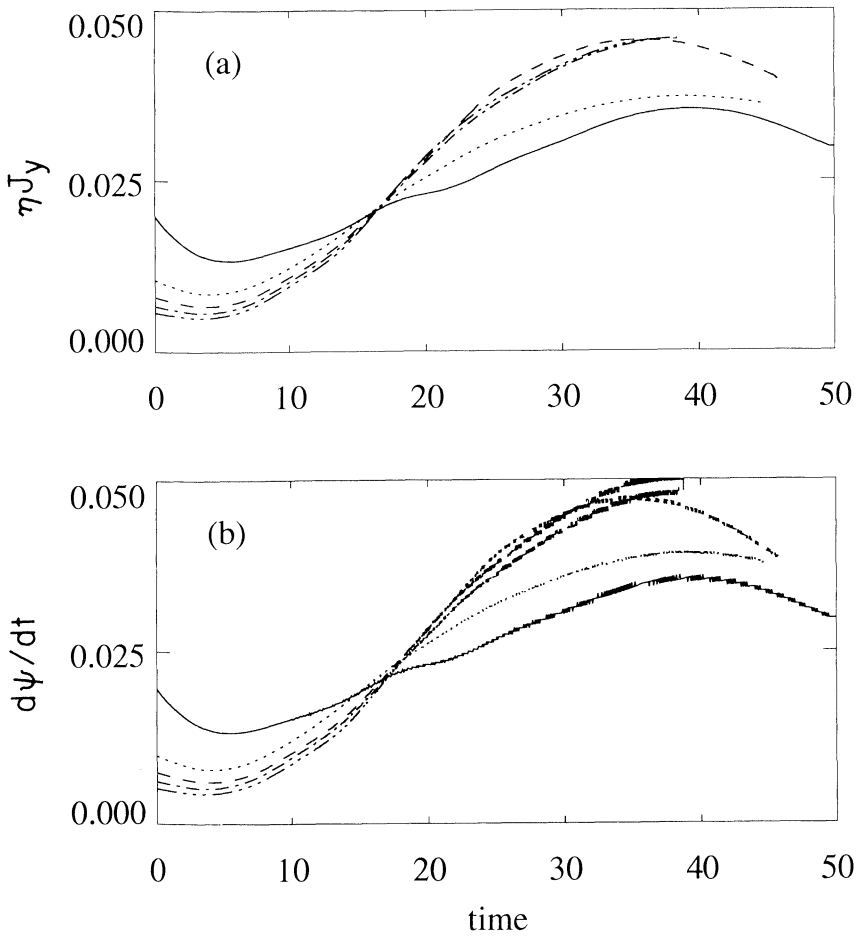

Figure 4. Reconnection electric field as a function of time calculated from (a) ηJ_y and (b) $d\psi/dt$ for initial condition 1 with $S = 100$, 200, 250, 300, and 350. The solid curve corresponds to $S = 100$, followed by $S = 200$ ($\cdots$), $S = 250$ (---), $S = 300$ ($-\cdot-$), and $S = 350$ ($-\cdots-$).

Plates 2a and 2b are quite comparable, there are significant qualitative differences. Specifically, we point to the development of localized regions of strong velocity shear (or vorticity) away from the reconnection layer in Plate 2b, not seen in Plate 2a. Intense current sheets are also seen to develop in these regions of strong velocity shear. In Plate 3 we plot the deviation from the equilibrium plasma density, defined by $\Delta\rho(x,z,t) \equiv \rho(x,z,t) - \rho(x,z,t=0)$ for initial condition 1 in the quasi-saturated regime (Plate 3a) and initial condition 2 at $t = 20$ (Plate 3b). The density depression near the neutral line in Plate 3b occurs over a significantly broader region and shows more structure than in Plate 3a. Density depletion layers have also been reported in the Hall MHD simulations of the GEM challenge by *Birn and Hesse* [this issue]; *Hesse et al.* [this issue], and *Shay et al.* [this issue]. While the formation of the depletion layer causes the run by Hesse et al. to terminate owing to a numerical instability, the run by Shay et al. is numerically stabilized by adding second-order diffusion terms to the time evolution equations for the density and pressure. Such depletion layers appear to be physically generated by the dynamics and are not numerical artifacts. The spatial location and time history of the depletion layers appear to vary from code to code, and these differences might be, in part, due to the differences in the generalized Ohm's law used in the various codes. Unless this tendency for depletion is damped by numerical means, it is extremely difficult to carry the simulation to saturation. Numerical damping in our time-stepping algorithm slows down the tendency for density depletion in the early stage of our run.

We now present the results of our damped runs. In Figure 5 we plot the electron and ion flow vectors at $t = 25$. By contrasting the electron and ion flow vectors in Figure 5 we see the separation between electron and ion flow channels that is a signature of Hall MHD reconnection with the electron flow significantly larger than the ion flow in the thin current sheet. In Plate 4 we present the contours of J_y, B_y, and the parallel current density and electric field at $t = 25$. Note that the B_y contours exhibit clear quadrupolar symmetry, also a signature of Hall MHD.

The reconnection rate, obtained by calculating ηJ_y at the X point, is shown as a function of time in Figure 6a. In Figure 6b the same reconnection rate is obtained from $E_y = d\psi/dt = \partial\psi/\partial t$. The hyperresistivity for

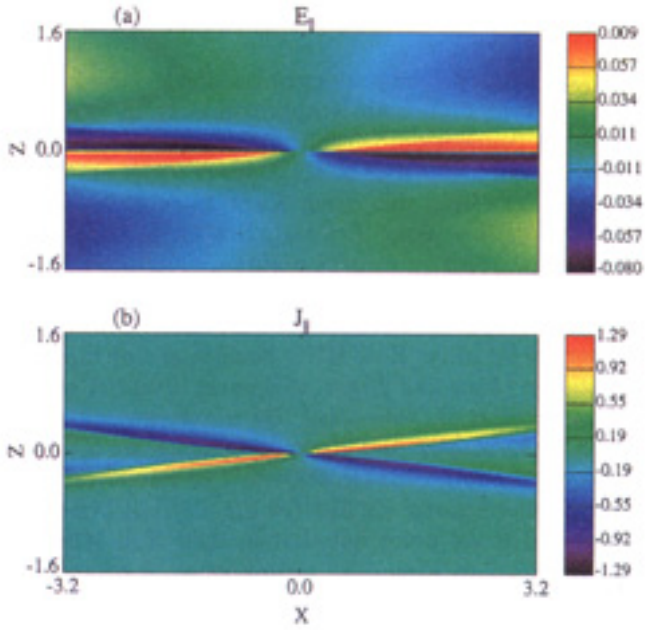

Plate 1. Contour plots for initial condition 1 at $t = 35$: (a) parallel electric field and (b) parallel current density.

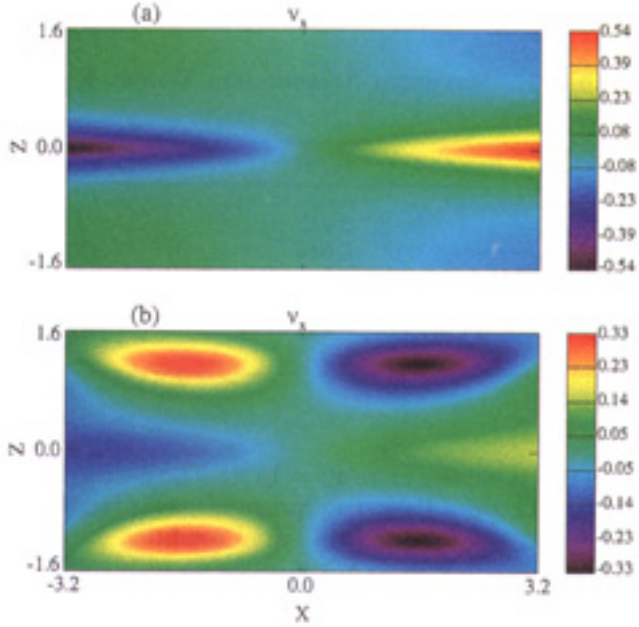

Plate 2. Contour plots of $v_x(x, z)$ without damping at $t = 25$ for (a) initial condition 1 and (b) initial condition 2.

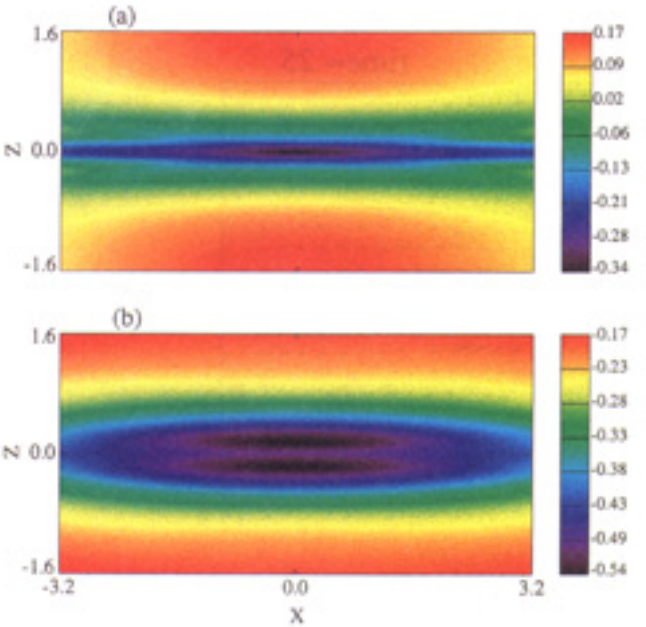

Plate 3. Contour plots of $\Delta\rho(x, z, t) \equiv \rho(x, z, t) - \rho(x, z, t = 0)$ without damping at $t = 20$ for (a) initial condition 1 and (b) initial condition 2.

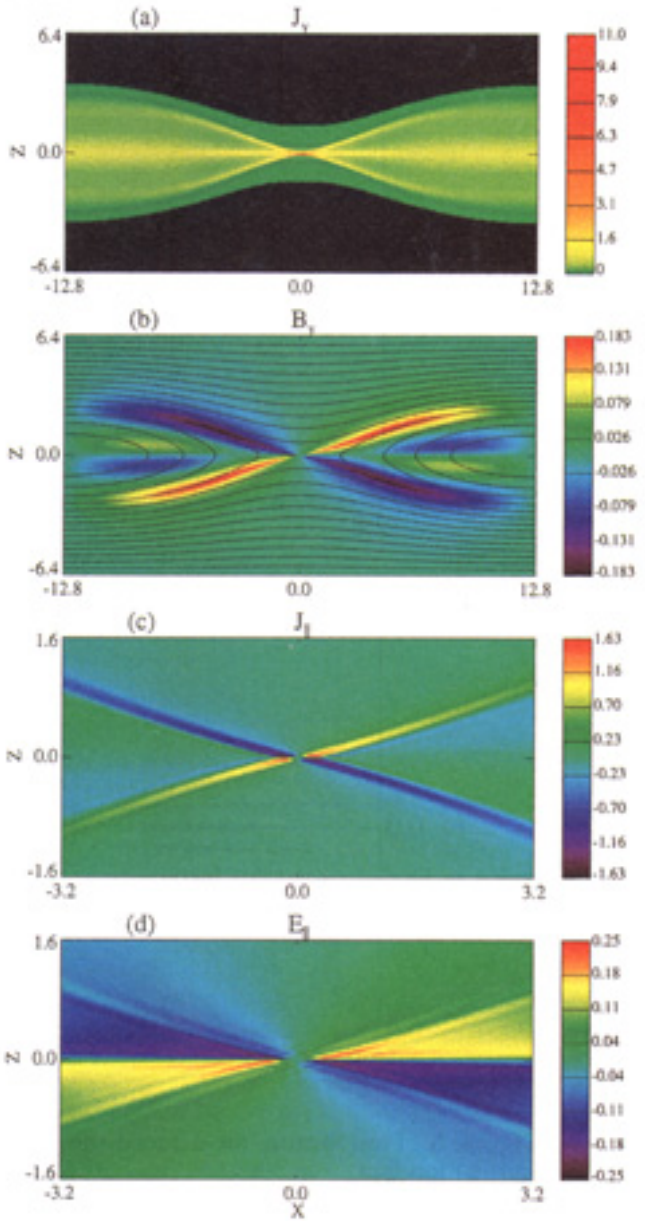

Plate 4. Contours for damped run with initial condition 2 at $t = 25$: (a) current J_y, (b) magnetic field B_y, (c) parallel current density, and (d) parallel electric field.

Table 1. Maximum Reconnection Electric Field for Initial Condition 1

S	$d\psi/dt$	ηJ_y
100	0.036	0.036
200	0.040	0.038
250	0.048	0.046
300	0.049	0.046
350	0.050	0.046

this run is chosen to be $\eta_h = 10^{-7}$. The numerical difference between these two computations is larger than that seen in Figure 2 with initial condition 1. As the thin current sheet with initial condition 2 is significantly more intense than that with initial condition 1, the effects of numerical diffusion and hyperresistivity are more significant in condition 2. Since other Hall MHD studies involved in the GEM challenge report the reconnection rate from computations $\partial\psi/\partial t$, we do the same for consistency. The peak reconnection electric field obtained from Figure 6b is approximately in agreement with the (dimensionless) value of 0.2 reported from PIC, hybrid, and other Hall MHD codes [*Birn et al.*, this issue; *Hesse et al.*, this issue; *Kuznetsova et al.*, this issue; *Otto*, this issue; *Prichett*, this issue; *Shay et al.*, this issue]. This agreement occurs despite the fact that the peak current density J_y in our simulations is about one order of magnitude larger than the current density reported by other Hall MHD simulations of the GEM challenge [*Birn and Hesse*, this issue; *Hesse et al.*, this issue; *Shay et al.*, this issue]. By comparing our results with those of *Birn and Hesse* [this issue], we infer that this is probably because the effect of numerical diffusion is significantly smaller for the UI Hall MHD run. Birn and Hesse point out that in their Hall MHD run (shown in their Figure 8), reconnection is governed by numerical dissipation rather than resistivity. Despite the larger values of the peak current density J_y in the UI code, the reconnection rate, ηJ_y, predicted by the code turns out to be close to the value obtained by Birn and Hesse, because the magnitude of the total η (phys-

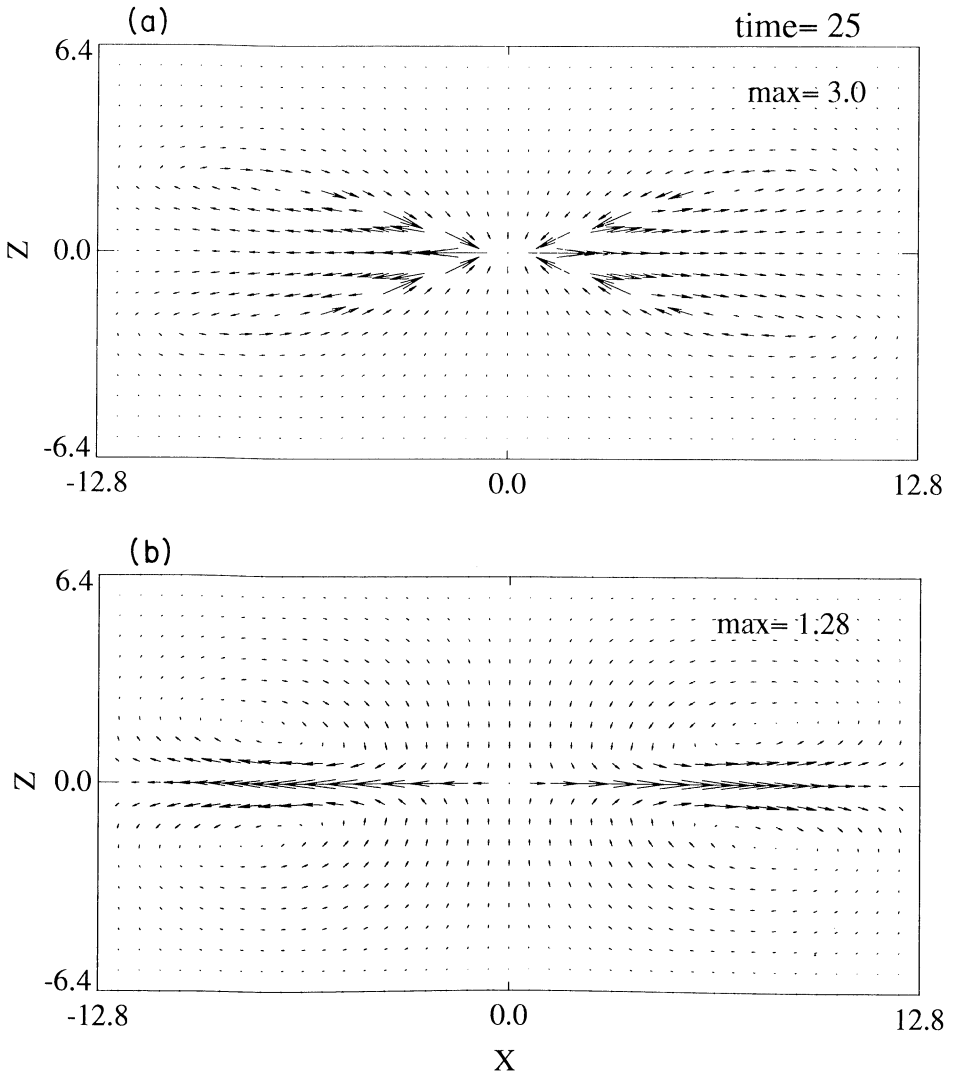

Figure 5. Flow vectors for damped run with initial condition 2 at $t = 25$ for (a) electron flow and (b) ion flow.

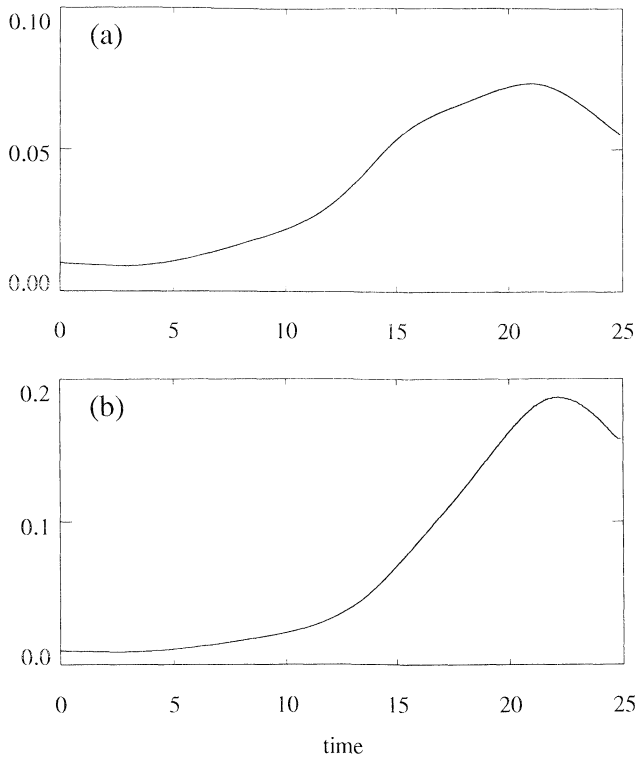

Figure 6. Reconnection electric field for intial condition 2 with $S = 200$ as a function of time calculated from (a) ηJ_y and (b) $\partial\psi/\partial t$.

ical plus numerical) is smaller in the UI code by nearly an order of magnitude. Note also that in contrast with *Hesse et al.* [this issue] and *Otto* [this issue], who use a localized, enhanced or current-dependent resistivity, we use a spatially uniform resistivity in all our runs.

5. Conclusions

The Hall MHD code developed at the University of Iowa produces results similar to PIC, hybrid, and other Hall MHD codes involved in the GEM challenge study. Since these codes span widely different levels of physical description ranging from the microscopic to the macroscopic, the quality of agreement gives us confidence that the essential physics of collisionless reconnection underlying these models are similar. In particular, all the GEM challenge studies reinforce the crucial role played by the Hall current in producing a reconnection rate that is weakly dependent on the mechanism that breaks field lines (resistivity or electron inertia).

We caution that the GEM challenge is a special case even within the restricted framework of two-dimensional collisionless reconnection models. Cases not covered by the GEM challenge are those in which (1) $B_y \neq 0$ in the initial stage, (2) the electron pressure is a tensor, and (3) reconnection is forced by boundary perturbations. We make some brief remarks on these three cases.

In case 1, when $B_y \geq B_0$ in the equilibrium state (equation (4)), Alfvén-whistler waves are replaced by kinetic Alfvén waves. Under these circumstances the electron pressure term in the generalized Ohm's law (equation (2)) enters on an equal footing with the Hall current term. A unified analytical treatment and numerical simulations encompassing both cases (that is, $B_y = 0$ as well as s $B_y \neq 0$) has been discussed elsewhere [*Wang et al.*, 2000].

In case 2, it is not necessary to invoke either resistivity or electron inertia as a mechanism for breaking field lines, because electron pressure tensor can support a parallel electric field at the X point [*Vasyliunas*, 1975; *Lyons and Pridemore-Brown*, 1990; *Cai et al.*, 1994; *Krauss-Varban and Omidi*, 1995; *Lin and Swift*, 1996; *Scudder*, 1997; *Kuznetsova et al.*, 1998; *Lottermoser et al.*, 1998].

In case 3, boundary perturbations play a significant rate in determining the time-history and magnitude of the reconnection rate. In the GEM challenge, reconnection is induced by imposing the large perturbation given by (11). This perturbation, which is largest at the origin, has been deliberately chosen so that all the codes attain a nonlinear quasi-saturated state quickly. While this is a reasonable strategy for code comparison, it is physically somewhat artificial. In many examples of physical interest, such as a magnetotail driven by a dawn-dusk electric field at the plasma sheet boundaries during the growth phase of a substorm [*Lee et al.*, 1985; *Birn and Hesse*, 1991; *Ma et al.*, 1995; *Pritchett and Coroniti*, 1995; *Bhattacharjee et al.*, 1998; *Ma and Bhattacharjee*, 1998], external perturbations are generally imposed at the boundaries of the system. The time evolution of a perturbation as it penetrates inward toward the separatrix and forces magnetic reconnection in a stable plasma is a problem of great physical interest and has been treated elsewhere analytically as well as numerically [*Wang et al.*, 1996; *Ma and Bhattacharjee*, 1996, 1998]. In such cases the plasma has been shown to exhibit multiple space scales and timescales during reconnection dynamics, not studied in the GEM challenge. A closely related problem is the so-called fast trigger problem [*Bhattacharjee et al*, 1999, and references therein].

Thus the GEM challenge should be viewed as a first step toward a more comprehensive picture even within the restrictive domain of two-dimensional reconnection phenomena. Furthermore, three-dimensional effects are likely to introduce even more drastic changes in the geometry as well as dynamics of reconnection.

Acknowledgments. We are indebted to J. D. Huba for suggesting and carrying out comparison tests with the NRL Hall MHD code. This research is supported by the NSF grant ATM-9529598 and NASA grants NAG5-3716 and NAG5-7883. Supercomputing resources were provided by the San Diego Supercomputing Center.

Janet G. Luhmann thanks Philip L. Pritchett and another referee for their assistance in evaluating this paper.

References

Bhattacharjee, and E. Hameiri, Self-consistent dynamo-like activity in turbulent plasmas, *Phys. Rev. Lett.*, *57*, 206 1986.

Bhattacharjee, A., Z. W. Ma, and X. Wang, Ballooning instability of a thin current sheet in the high-Lundquist-number magnetotail, *Geophys. Res. Lett., 25,* 861, 1998.

Bhattacharjee, A., Z. W. Ma, and X. Wang, Impulsive reconnection dynamics in collisionless laboratory and space plasmas, *J. Geophys. Res., 104,* 14,543, 1999.

Birn, J., and M. Hesse, The substorm current wedge and field-aligned currents in MHD simulations of magnetotail reconnection, *J. Geophys. Res., 96,* 1611, 1991.

Birn, J., and M. Hesse, Global Environment Modeling (GEM) magnetic reconnection challenge: Resistive tearing, anisotropic pressure, and Hall effects, *J. Geophys. Res.,* this issue.

Birn, J., et al., Global Environment Modeling (GEM) magnetic reconnection challenge, *J. Geophys. Res.,* this issue.

Biskamp, D., *Nonlinear Magnetohydrodynamics*, Cambridge Univ. Press, New York, 1993.

Biskamp, D., E. Schwarz, and J. F. Drake, Two-fluid theory of collisionless magnetic reconnection, *Phys. Plasmas, 4,* 1002, 1997.

Boozer, A., Ohm's law for mean magnetic fields, *J. Plasma Phys., 35,* 133, 1986.

Brio, M., and C. C. Wu, An upward finite-differencing scheme for the equations of ideal magnetohydrodynamics, *J. Comput. Phys., 75,* 400, 1988.

Cai, H. J., D. Q. Ding, and L. C. Lee, Momentum transport near a magnetic X line in collisionless reconnection, *J. Geophys. Res., 99,* 35, 1994.

Drake, J. F., R. G. Kleva, and M. E. Mandt, Structure of thin current layers: Implications for magnetic reconnection, *Phys. Rev. Lett., 73,* 1251, 1994.

Hesse, M., K. Schindler, J. Birn, and M. Kuznetsova, The diffusion region in collisionless magnetic reconnection, *Phys. Plasmas, 5,* 1781, 1999.

Hesse, M., J. Birn, and M. Kuznetsova, Collisionless magnetic reconnection: Electron processes and transport modeling, *J. Geophys. Res.,* this issue.

Huba, J. D., and J. G. Lyon, A new 3D MHD algorithm: The distribution function method, *J. Plasma Phys., 61,* 391, 1999.

Krauss-Varban, D., and N. Omidi, Large-scale hybrid simulations of the magnetotail during reconnection, *Geophys. Res. Lett., 22,* 3271, 1995.

Kuznetsova, M., M. Hesse, and D. Winske, Kinetic quasi-viscous and bulk flow inertia effects in collisionless magnetotail reconnection, *J. Geophys. Res., 103,* 199, 1998.

Kuznetsova, M., M. Hesse, and D. Winske, Collisionless reconnection supported by nongyrotropic pressure effects in hybrid and particle simulations, *J. Geophys. Res.,* this issue.

Lee, L. C., Z. F. Fu, and S.-I. Akasofu, A simulation study of forced reconnection processes and magnetospheric storms and substorm, *J. Geophys. Res., 90,* 10,896, 1985.

Lin, Y., and D. W. Swift, A two-dimensional hybrid simulation of magnetotail reconnection layer, *J. Geophys. Res., 101,* 19,859, 1996.

Lottermoser, R.-F., M. Scholer, and A. P. Mathews, Ion kinetic effects in magnetic reconnection: Hybrid simulations, *J. Geophys. Res., 103,* 4547, 1998.

Lyons, L. R., and D. C. Pridemore-Brown, Force balance near an X line in a collisionless plasmas, *J. Geophys. Res., 95,* 20,903, 1990.

Ma, Z. W., and A. Bhattacharjee, Fast impulsive reconnection and current sheet intensification due to electron pressure gradients in semi-collisional plasmas, *Geophys. Res. Lett., 23,* 1673, 1996.

Ma, Z. W., and A. Bhattacharjee, Sudden enhancement and disruption of thin current sheets in the magnetotail due to electron pressure gradients, *Geophys. Res. Lett., 25,* 3277, 1998.

Ma, Z. W., X. Wang, and A. Bhattacharjee, Growth, sudden enhancement, and relaxation of current sheets in the magnetotail: Two-dimensional substorm dynamics, *Geophys. Res. Lett., 22,* 2985, 1995.

Mandt, M. E., R. E. Denton, and J. F. Drake, Transition to whistler-mediated magnetic reconnection, *Geophys. Res. Lett., 21,* 73, 1994.

Otto, A., Geospace Environment Modeling (GEM) magnetic reconnection challenge: MHD and Hall MHD-constant and current dependent resistivity models, *J. Geophys. Res.,* this issue.

Pritchett, P. L., Geospace Environment Modeling (GEM) magnetic reconnection challenge: Simulations with a full particle electromagnetic code, *J. Geophys. Res.,* this issue.

Pritchett, P. L., and F. V. Coroniti, Formation of thin current sheets during plasma sheet convection, *J. Geophys. Res., 100,* 23,551, 1995.

Scudder, J. D., Theoretical approaches to the description of magnetic merging: The need for finite β_e, anisotropic, ambipolar Hall MHD, *Space Sci. Rev., 80,* 235, 1997.

Shay, M. A., and J. F. Drake, The role of electron dissipation on rate of collisionless magnetic reconnection, *Geophys. Res. Lett., 25,* 3759, 1998.

Shay, M. A., J. F. Drake, B. N. Rogers, and R. E. Denton, Alfvénic collisionless magnetic reconnection and the Hall term, *J. Geophys. Res.,* this issue.

Sonnerup, B. U. O., Magnetic field reconnection, in *Solar System Plasma Physics*, edited by L. J. Lanzerotti, C. F. Kennel, and E. N. Parker, vol. 3, p. 46, North-Holland, New York, 1979.

Strauss, H. R., Hyperresistivity produced by tearing mode turbulence, *Phys. Fluids, 29,* 3668, 1986.

Terasawa, T., Hall current effect on tearing mode instability, *Geophys. Res. Lett., 10,* 475, 1983.

Vasyliunas, V. M., Theoretical models of magnetic field line merging, *Rev. Geophys., 13,* 303, 1975.

Wang, X., Z. W. Ma, and A. Bhattacharjee, Fast magnetic reconnection and sudden enhancement of current sheet due to inward boundary flow, *Phys. Plasmas, 3,* 2129, 1996.

Wang, X., A. Bhattacharjee, and Z. W. Ma, Collisionless reconnection: Effects of Hall current and electron pressure gradient, *J. Geophys. Res.,* in press, 2000.

A. Bhattacharjee and Z. W. Ma, Department of Physics and Astronomy, 203 Van Allen Hall, University of Iowa, City, IA 52242-1479. (e-mail:abhattac@newton.physics.uiowa.edu)

(Received August 9, 1999; revised March 24, 2000; accepted April 6, 2000.)